A Transient Simulation to Predict the Kinetic Behavior of Hydrogels Responsive to Electric Stimulus

Hua Li,* Jun Chen, and K. Y. Lam

Institute of High Performance Computing, National University of Singapore, 1 Science Park Road, #01-01 The Capricorn, Singapore Science Park II, Singapore 117528

A kinetic analysis of the response of electric-sensitive hydrogels to an externally applied electric field is conducted for the first time through modeling and transient simulation. This model, called the multieffect coupling electric stimulus (MECe), considers the effects of multiphases and multiphysics. Its extended application to transient simulation is validated against available experimental data, and good agreement is achieved. The concentration kinetics of ionic species is simulated. The simulation predicts the kinetic behavior of the hydrogels with consideration of the influences of important parameters such as the electric potential, fixed-charge density, bath solution concentration, and hydrogel average curvature.

Introduction

In essence, a hydrogel is hydrophilic mixture consisting of three-dimensional cross-linked polymeric network and interstitial water or biological fluid, such that the hydrogel exhibits both solidlike and liquidlike properties. A stimuli-responsive hydrogel is often created if an ionic monomer is incorporated into the hydrogel network. The resulting charged group is generally called fixed charge, since its mobility is much less than that of freely mobile ions within the interstitial fluid. The responsive hydrogel is thus a multiphase mixture. As shown in Figure 1, it consists of solid phase (polymeric network matrix with fixed charge), fluid phase (interstitial water), and ion phase (mobile ionic species).

Hydrogels are widely employed in biomaterial-related fields not only because of their excellent biocompatibility and biostability characteristics, which can be tailored, but also because they are relatively inexpensive. Lately, due to the sensitivity of the stimuli-responsive hydrogels to a wide variety of surrounding environmental conditions such as applied electric field, solution pH, temperature, and chemicals, their applications as active elements in BioMEMS have been explored intensively in areas such as controlled drug release, microscale actuators/sensors, microfluidic flow control, and filtration/separation processes.[1−3] Furthermore, literature search also reveals that several efforts were made to develop mathematical models for numerical prediction of the behavior of the hydrogels responding to various stimuli,[4−13] though most studies of the stimuli-responsive hydrogels were experimentally based.

Even though there are several research works detailing the experimental and theoretical studies concerning the electric-sensitive hydrogels, the responsive characteristics of these hydrogels remain poorly understood. Few theoretical modeling studies are found in open literature. They include the early biphase model developed by Mow et al.,[14] the swelling thermo-analogue theory by Myers et al.,[15] the bicomponent theory by Lanir,[16] and the electromechanical theory by Eisenberg and Grodzinsky.[17] These mathematical models are generally unable to work well due to their exclusion of some important physical parameters such as the fixed-charge density and diffusive ionic concentrations. To overcome the drawbacks, Lai et al.[18]
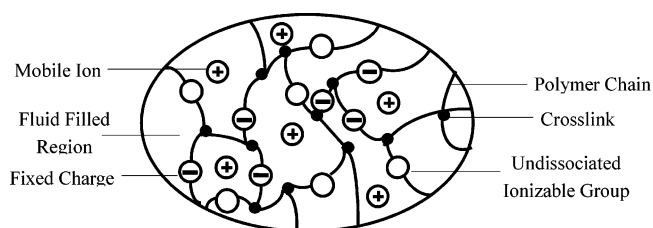

Figure 1. Microscopic structure of the charged hydrogel.

proposed a triphase mechanoelectrochemical theory for the responsive behavior of hydrogel-like tissues by constructing a theoretical bridge between physical chemistry and continuum mixture theory and incorporating the chemical potential whose gradient is employed as the driving force for fluid flow and ion transport. This triphase theory represents a significant progression in the modeling development of hydrogels or hydrogel-like tissues. Recently, Wallmersperger et al.[19] and Zhou et al.[20] put forward the models to simulate the deformation of electric-sensitive hydrogels under an external electric field. However, the models still have limited application. For example, in the model developed by Wallmersperger et al.,[19] Newton's second law is directly used as the mechanical governing equation. This results in difficulty describing the mechanical behavior of multiphase hydrogels. In the model by Zhou et al.,[20] the electroneutrality condition is required. Computational domain is also limited within the interior hydrogel, excluding the externally surrounding bath solution. On the basis of the multiphase theory, the present authors have developed a novel mathematical model,[21] termed the multieffect coupling electric stimulus (MECe) model, for simulation of responsive behaviors of electric-sensitive hydrogels when immersed into a bath solution subject to externally applied electric field. This model has been validated to perform well in steady-state simulation to predict the equilibrium of the hydrogels.[22]

In this paper, the MECe model will be further applied to transient simulation to study the kinetic behavior of the hydrogels. The MECe model, consisting of nonlinear coupled partial differential governing equations, is first described. Numerical comparison is made between the computed results and experimental data extracted from open literature. Then, the transient simulations are carried out for discussion of the concentration kinetics of diffusive ionic species and the effects of important parameters, including the electric potential, fixed-

* Corresponding author. Tel: +65-64191249. Fax: +65-64191280. E-mail address: lihua@ihpc.a-star.edu.sg.

CDV

charge density, bath solution concentration, and hydrogel average curvature, on the kinetic behavior of the electric-stimulus responsive hydrogels.

Developed MECe Model

Transient Governing Equations of the MECe Model. On the basis of the MECe model,[21,22] the transient governing equations can be expressed by the following:

Nernst−Planck diffusion equation for the kth ionic concentration c^k

$$\frac{\partial c_k}{\partial t} = (D_k c^k_{,i})_{,i} + \frac{F_c z^k}{RT}(D_k c^k \psi_{,i})_{,i} \quad (k = 1, 2, \dots n_f) \quad (1)$$

Poisson equation for the electric potential ψ

$$\nabla^2 \psi = -\frac{F_c}{\epsilon \epsilon_0}\sum_{k=1}^{n_f}(z^k c^k + z^f c^f) \quad (2)$$

the continuity and momentum equations of the mixture phase for the fluid pressure p and hydrogel displacement u

$$\nabla \frac{\partial u}{\partial t} = \nabla\left[\frac{(\phi^w)^2}{f_{ws}}(\nabla p + RT\nabla\sum_k(1-\Phi^k)c^k + F_c\sum_k z^k c^k\nabla\psi)\right] \quad (3)$$

$$\nabla\cdot(-p\mathbf{I} + \lambda_s tr(\mathbf{E})\mathbf{I} + 2\mu_s\mathbf{E}) = 0 \quad (4)$$

the constitutive equations for fixed-charge density c^f and volume fraction of water phase ϕ^w

$$c^f = \frac{c_0^f}{[1 + tr(\mathbf{E})/\phi_0^w]} \quad \phi^w = 1 - \frac{\phi_0^s}{[1 + tr(\mathbf{E})]} \quad (5)$$

where D_k, c^k, and z^k are the diffusive coefficient, concentration, and valence of kth ion species, respectively. F_c is the Faraday constant, R is the universal gas constant, T is the absolute temperature, ψ is the electric potential, ϵ is the dielectric constant, and ϵ_0 is the permittivity of free space. c^f and z^f are the density and valence of the fixed-charge group, respectively. ϕ^w is the volume fraction of water phase, f_{ws} is the diffusive drag coefficient between solid and water phases, Φ^k is the osmotic coefficient of the kth ion species, p is the fluid pressure, and $\mathbf{I}$ is the identity tensor. u and $\mathbf{E}$ are the displacement and elastic strain vector of the solid matrix phase, respectively. λ_s and μ_s are Lamé coefficients of solid matrix. c_0^f, ϕ_0^s, and ϕ_0^w are the fixed-charge density and volume fractions of solid and water phases at reference configuration, respectively.

For convenience of numerical simulations, a set of nondimensional variables is defined as

$$\bar{\zeta} = \frac{\zeta}{L_{ref}} \quad \bar{u} = \frac{u}{L_{ref}} \quad (6)$$

$$\bar{c}_k = \frac{c_k}{c_{ref}} \quad \bar{c}_f = \frac{c_f}{c_{ref}} \quad (7)$$

$$\bar{\psi} = \frac{\psi}{\psi_{ref}} = \frac{F\psi}{\alpha RT} \quad (8)$$

$$\bar{p} = \frac{p}{p_{ref}} = \frac{p}{\beta c_{ref}RT} \quad (9)$$

where ζ denotes the spatial coordinate variable. α and β are weighted coefficients. L_{ref}, c_{ref}, ψ_{ref}, and p_{ref} are the characteristic length, concentration, electric potential, and pressure, respectively.

Substituting the definitions of the nondimensional variables (eqs 6−9) into the transient governing eqs 1−4 of the MECe model, the nondimensional forms of the partial differential governing equations are obtained as

$$L_{ref}^2\frac{\partial \bar{c}_k}{\partial t} = (D_k\bar{c}^k_{,i})_{,i} + \alpha z^k(D_k\bar{c}^k\bar{\psi}_{,i})_{,i} \quad (k = 1, 2, \dots n_f) \quad (10)$$

$$\nabla^2\bar{\psi} = -\frac{F_c^2 L_{ref}^2 c_{ref}}{\epsilon\epsilon_0 RT\alpha}\sum_{k=1}^{n_f}(z^k\bar{c}^k + z^f\bar{c}^f) \quad (11)$$

$$\frac{L_{ref}^2}{c_{ref}RT}\nabla\frac{\partial\bar{u}}{\partial t} =$$
$$\nabla\left[\frac{(\phi^w)^2}{f_{ws}}(\beta\nabla\bar{p} + RT\nabla\sum_k(1-\Phi^k)\bar{c}^k + \alpha\sum_k z^k\bar{c}^k\nabla\bar{\psi})\right] \quad (12)$$

$$\beta RT c_{ref}\nabla\cdot(p\mathbf{I}) = \nabla[\lambda_s tr(\mathbf{E})\mathbf{I} + 2\mu_s\mathbf{E}] \quad (13)$$

It is noted that only one-dimensional (1-D) numerical simulations as preliminary work are carried out in this paper. As shown in Figure 2, an electric-sensitive hydrogel strip is immersed into ideal NaCl solution subject to an externally applied electric field. Thus, only displacement along the x direction is computed. It is also assumed that one of two edge points a and b in the thickness h direction is fixed to eliminate rigid body displacement. The set of the governing eqs 10−13 is thus reduced to the nondimensional 1-D partial differential transient governing equations of the MECe model as follows:

$$L_{ref}^2\frac{\partial\bar{c}^k}{\partial t} = D_k\left(\frac{\partial^2\bar{c}^k}{\partial\bar{x}^2} + \alpha z^k\frac{\partial\bar{c}^k}{\partial\bar{x}}\frac{\partial\bar{\psi}}{\partial\bar{x}} + \alpha z^k\bar{c}^k\frac{\partial^2\bar{\psi}}{\partial\bar{x}^2}\right) \quad (k = +, -) \quad (14)$$

$$\frac{\partial^2\bar{\psi}}{\partial\bar{x}^2} + \frac{F_c^2 L_{ref}^2 c_{ref}}{\epsilon\epsilon_0 RT\alpha}\left(\sum_{k=+,-}z^k\bar{c}^k + z^f\bar{c}^f\right) = 0 \quad (15)$$

$$(3\lambda_s + 2\mu_s)\frac{\partial^2\bar{u}}{\partial\bar{x}^2} - \beta RT c_{ref}\frac{\partial\bar{p}}{\partial\bar{x}} = 0 \quad (16)$$

$$\frac{L_{ref}^2 f_{ws}}{c_{ref}RT}\frac{\partial}{\partial t}\left(\frac{\partial\bar{u}}{\partial\bar{x}}\right) = \beta\left(\phi^w\frac{\partial^2\bar{p}}{\partial\bar{x}^2} + 2\frac{\partial\phi^w}{\partial\bar{x}}\frac{\partial\bar{p}}{\partial\bar{x}}\right) +$$
$$\alpha\left\{2\frac{\partial\phi^w}{\partial\bar{x}}\frac{\partial\bar{\psi}}{\partial\bar{x}}\sum_{k=+,-}z^k\bar{c}^k + \phi^w\left[\frac{\partial\bar{\psi}}{\partial\bar{x}}\sum_{k=+,-}\left(z^k\frac{\partial\bar{c}^k}{\partial\bar{x}}\right) + \frac{\partial^2\bar{\psi}}{\partial\bar{x}^2}\sum_{k=+,-}z^k\bar{c}^k\right]\right\} \quad (17)$$

Boundary and Initial Conditions. The present computational domain of the diffusive ionic concentrations $\bar{c}^k$ and electric potential $\bar{\psi}$ for eqs 14 and 15 covers both the hydrogel and the surrounding bath solution. As such, the boundary conditions of the unknown $\bar{c}^k$ and $\bar{\psi}$ are imposed at the two electrodes fixed at the ends of bath solution (see Figure 2),

$$\bar{c}|_{anode} = \bar{c}|_{cathode} = \bar{c}^* \quad (18)$$

$$\bar{\psi}|_{anode} = 0.5\bar{V}_e \quad \text{and} \quad \bar{\psi}|_{cathode} = -0.5\bar{V}_e \quad (19)$$

where $\bar{c}^*$ is the initial salt concentration of the bath solution and $\bar{V}_e$ is the applied voltage.
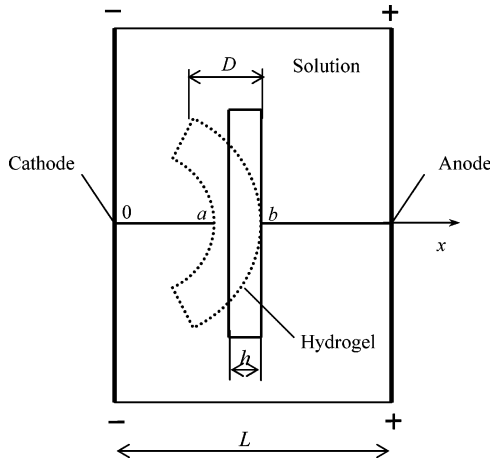
CDV

Figure 2. Diagram of a hydrogel strip immersed in bath solution under applied electric field.

However, the computational domain of the fluid pressure $\bar{p}$ and hydrogel displacement $\bar{u}$ for eqs 16 and 17 covers the hydrogel region only. The corresponding boundary conditions are required at the two hydrogel−solution interfaces. On the basis of the assumption that, at equilibrium state, the chemical potentials of water and ion phases inside the hydrogels should be equal to those outside the hydrogels, the boundary condition of the fluid pressure $\bar{p}$ at the hydrogel−solution interfaces is given as

$$\bar{p}_{\text{interface}} = RT(\bar{c}_{\text{in−interface}}^+ + \bar{c}_{\text{in−interface}}^- - \bar{c}_{\text{out−interface}}^+ - \bar{c}_{\text{out−interface}}^-) - p_0 \quad (20)$$

where $\bar{c}_{\text{in−interface}}^k$ ($k = +, -$) are the ionic concentrations within the hydrogels near the interfaces, $\bar{c}_{\text{out−interface}}^k$ ($k = +, -$) are the ionic concentrations within the surrounding bath solution near the interfaces, and p_0 denotes the fluid pressure at reference configuration. Due to the mechanical equilibrium of the mixture phase, the boundary condition of the hydrogel displacement $\bar{u}$ at the hydrogel−solution interface is given as

$$(3\lambda_s + 2\mu_s)\frac{\partial \bar{u}_{\text{interface}}}{\partial \bar{x}} = \beta RTc_{\text{ref}} \bar{p}_{\text{interface}} \quad (21)$$

For implementation of transient simulation to predict the kinetic response of the electric-sensitive hydrogels, initial conditions are also required. It is assumed here that the hydrogel is initially in the equilibrium state under the effect of bath solution only, when the external electric field is not applied. This equilibrium state is taken as the initial condition for transient simulation. Corresponding steady-state computations can thus give the values used as the initial conditions as

$$\bar{c}_{\text{initial}}^{\text{transient}} = \bar{c}_{\nu=0}^{\text{steady}} \quad (22)$$

$$\bar{\psi}_{\text{initial}}^{\text{transient}} = \bar{\psi}_{\nu=0}^{\text{steady}} \quad (23)$$

$$\bar{p}_{\text{initial}}^{\text{transient}} = \bar{p}_{\nu=0}^{\text{steady}} \quad (24)$$

$$\bar{u}_{\text{initial}}^{\text{transient}} = \bar{u}_{\nu=0}^{\text{steady}} \quad (25)$$

where $\bar{c}_{\nu=0}^{\text{steady}}$, $\bar{\psi}_{\nu=0}^{\text{steady}}$, $\bar{p}_{\nu=0}^{\text{steady}}$, and $\bar{u}_{\nu=0}^{\text{steady}}$ represent the steady-state computational results without the externally applied electric field.

Discretization of Transient Governing Equations of the MECe Model. A strong-form meshless numerical technique called Hermite-cloud method (HCM)[23,24] is employed for transient solution of the nonlinear coupled partial differential governing eqs 14−17 of the MECe model. The method constructs the Hermite-type interpolation functions and uses the point collocation technique for discretization of partial differential equations to directly compute the approximate solutions of both unknown functions and first-order derivatives[23,24]

$$\tilde{f}(x, y) = \sum_{n=1}^{N_T} N_n(x, y)f_n + \sum_{m=1}^{N_S}\left[x - \sum_{n=1}^{N_T} N_n(x, y)x_n\right]M_m(x, y)g_{xm} + \sum_{m=1}^{N_S}\left[y - \sum_{n=1}^{N_T} N_n(x, y)y_n\right]M_m(x, y)g_{ym} \quad (26)$$

On the basis of the θ-weighted finite difference scheme,[25] eq 14 is discretized first in time t domain

$$\bar{c}_{(n+1)}^k - \bar{c}_{(n)}^k = \frac{\Delta t D_k}{L_{\text{ref}}^2}\left[\theta\left(\frac{\partial^2 \bar{c}_{(n+1)}^k}{\partial \bar{x}^2} + \alpha z^k \frac{\partial \bar{c}_{(n+1)}^k}{\partial \bar{x}}\frac{\partial \bar{\psi}_{(n+1)}}{\partial \bar{x}} + \alpha z^k \bar{c}_{(n+1)}^k \frac{\partial^2 \bar{\psi}_{(n+1)}}{\partial \bar{x}^2}\right) + (1-\theta)\left(\frac{\partial^2 \bar{c}_{(n)}^k}{\partial \bar{x}^2} + \alpha z^k \frac{\partial \bar{c}_{(n)}^k}{\partial \bar{x}}\frac{\partial \bar{\psi}_{(n)}}{\partial \bar{x}} + \alpha z^k \bar{c}_{(n)}^k \frac{\partial^2 \bar{\psi}_{(n)}}{\partial \bar{x}^2}\right)\right] \quad (27)$$

where the subscript n denotes time $t = t_n$ and $\Delta t = t_{n+1} - t_n$ represents a time step. θ is a weighted coefficient, and it is defined as $0.5 < \theta < 1.0$ for the computational stability condition.[25]

By using the HCM, eq 27 is further approximated in spatial domain in the discrete form as

$$\sum_{j=1}^{np} N_j(\bar{x}_i)\bar{c}_{j(n+1)}^k - \sum_{m=1}^{np}\left[\bar{x}_i - \sum_{j=1}^{np} N_j(\bar{x}_i)\bar{x}_j\right]M_m(\bar{x}_i)\bar{c}_{xm(n+1)} - \frac{\Delta t D_k \theta}{L_{\text{ref}}^2}\left\{\sum_{j=1}^{np} N_{xxj}(\bar{x}_i)\bar{c}_{j(n+1)}^k + \alpha z^k \sum_{m=1}^{np} M_m(\bar{x}_i)\bar{c}_{xm(n+1)}^k \sum_{m=1}^{np} M_m(\bar{x}_i)\bar{\psi}_{xm(n+1)} + \alpha z^k \sum_{j=1}^{np} N_{xxj}(\bar{x}_i)\bar{\psi}_{j(n+1)}\left[\sum_{j=1}^{np} N_j(\bar{x}_i)\bar{c}_{j(n+1)}^k - \sum_{m=1}^{np}\left(\bar{x}_i - \sum_{j=1}^{np} N_j(\bar{x}_i)\bar{x}_j\right)M_m(\bar{x}_i)\bar{c}_{xm(n+1)}\right]\right\} = \sum_{j=1}^{np} N_j(\bar{x}_i)\bar{c}_{j(n)}^k - \sum_{m=1}^{np}\left(\bar{x}_i - \sum_{j=1}^{np} N_j(\bar{x}_i)\bar{x}_j\right)M_m(\bar{x}_i)\bar{c}_{xm(n)} + \frac{\Delta t D_k(1-\theta)}{L_{\text{ref}}^2}\left\{\sum_{j=1}^{np} N_{xxj}(\bar{x}_i)\bar{c}_{j(n)}^k + \alpha z^k \sum_{m=1}^{np} M_m(\bar{x}_i)\bar{c}_{xm(n)}^k \sum_{m=1}^{np} M_m(\bar{x}_i)\bar{\psi}_{xm(n)} + \alpha z^k\left[\sum_{j=1}^{np} N_j(\bar{x}_i)\bar{c}_{j(n)}^k - \sum_{m=1}^{np}\left(\bar{x}_i - \sum_{j=1}^{np} N_j(\bar{x}_i)\bar{x}_j\right)M_m(\bar{x}_i)\bar{c}_{xm(n)}\right]\sum_{j=1}^{np} N_{xxj}(\bar{x}_i)\bar{\psi}_{j(n)}\right\} \quad (28)$$

Similarly, eqs 15−17 can also be discretized in both time and spatial domains in the following approximate form

CDV

$$\sum_{j=1}^{np} N_{xxj}(\bar{x}_i)\bar{\psi}_{j(n+1)} + \frac{F_c^2 L_{ref}^2 c_{ref}}{\epsilon\epsilon_0 RT\alpha}\left\{ z^f\bar{c}^f + \right.$$

$$\sum_{k=+,-} z^k\left[\sum_{j=1}^{np} N_j(\bar{x}_i)\bar{c}_{j(n+1)}^k - \right.$$

$$\left.\left.\sum_{m=1}^{np}\left(\bar{x}_i - \sum_{j=1}^{np} N_j(\bar{x}_i)\bar{x}_j\right)M_m(\bar{x}_i)\bar{c}_{xm(n+1)}\right]\right\} = 0 \quad (29)$$

$$(3\lambda_s + 2\mu_s)\sum_{j=1}^{npGel} N_{xxj}(\bar{x}_i)\bar{u}_{j(n+1)} - \beta RT c_{ref}\sum_{m=1}^{npGel} M_m(\bar{x}_i)\bar{p}_{xm(n+1)} = 0 \quad (30)$$

$$\frac{L_{ref}^2 f_{ws}}{c_{ref}RT}\sum_{m=1}^{npGel} M_m(\bar{x}_i)\bar{u}_{xm(n+1)} -$$

$$\Delta t\theta\beta\left[\phi^w\sum_{j=1}^{npGel} N_{xxj}(\bar{x}_i)\bar{p}_{j(n+1)} + 2\frac{\partial\phi^w}{\partial\bar{x}}\sum_{m=1}^{npGel} M_m(\bar{x}_i)\bar{p}_{xm(n+1)}\right] -$$

$$\alpha\Delta t\theta\left\{2\frac{\partial\phi^w}{\partial\bar{x}}[\sum_{m=1}^{npGel} M_m(\bar{x}_i)\bar{\psi}_{xm(n+1)}] \times\right.$$

$$\left[\sum_{k=+,-} z^k\sum_{j=1}^{npGel}\left(N_j(\bar{x}_i)\bar{c}_{j(n+1)}^k - \right.\right.$$

$$\left.\left.\sum_{m=1}^{npGel}\left(\bar{x}_i - \sum_{j=1}^{npGel} N_j(\bar{x}_i)\bar{x}_j\right)M_m(\bar{x}_i)\bar{c}_{xm(n+1)}\right)\right] +$$

$$\phi^w\left[\sum_{m=1}^{npGel} M_m(\bar{x}_i)\bar{\psi}_{xm(n+1)}\left(\sum_{k=+,-} z^k\sum_{m=1}^{npGel} M_m(\bar{x}_i)\bar{c}_{xm(n+1)}^k\right) + \right.$$

$$\sum_{j=1}^{npGel} N_{xxj}(\bar{x}_i)\bar{\psi}_{j(n+1)}\sum_{k=+,-} z^k\sum_{j=1}^{npGel}\left(N_j(\bar{x}_i)\bar{c}_{j(n+1)}^k - \right.$$

$$\left.\left.\left.\sum_{m=1}^{npGel}\left(\bar{x}_i - \sum_{j=1}^{npGel} N_j(\bar{x}_i)\bar{x}_j\right)M_m(\bar{x}_i)\bar{c}_{xm(n+1)}\right)\right]\right] =$$

$$\frac{L_{ref}^2 f_{ws}}{c_{ref}RT}\sum_{m=1}^{npGel} M_m(\bar{x}_i)\bar{u}_{xm(n)} +$$

$$\Delta t(1-\theta)\beta\left[\phi^w\sum_{j=1}^{npGel} N_{xxj}(\bar{x}_i)\bar{p}_{j(n)} + 2\frac{\partial\phi^w}{\partial\bar{x}}\sum_{m=1}^{npGel} M_m(\bar{x}_i)\bar{p}_{xm(n)}\right] + \alpha\Delta t$$

$$(1-\theta)\left\{2\frac{\partial\phi^w}{\partial\bar{x}}\left[\sum_{m=1}^{npGel} M_m(\bar{x}_i)\bar{\psi}_{xm(n)}\right] \times\right.$$

$$\left[\sum_{k=+,-} z^k\sum_{j=1}^{npGel}\left(N_j(\bar{x}_i)\bar{c}_{j(n)}^k - \right.\right.$$

$$\left.\left.\sum_{m=1}^{npGel}\left(\bar{x}_i - \sum_{j=1}^{npGel} N_j(\bar{x}_i)\bar{x}_j\right)M_m(\bar{x}_i)\bar{c}_{xm(n)}\right)\right] +$$

$$\phi^w\left[\sum_{m=1}^{npGel} M_m(\bar{x}_i)\bar{\psi}_{xm(n)}\left(\sum_{k=+,-} z^k\sum_{m=1}^{npGel} M_m(\bar{x}_i)\bar{c}_{xm(n)}^k\right) + \right.$$

$$\sum_{j=1}^{npGel} N_{xxj}(\bar{x}_i)\bar{\psi}_{j(n)}\sum_{k=+,-} z^k\sum_{j=1}^{npGel}\left(N_j(\bar{x}_i)\bar{c}_{j(n)}^k - \right.$$

$$\left.\left.\left.\sum_{m=1}^{npGel}\left(\bar{x}_i - \sum_{j=1}^{npGel} N_j(\bar{x}_i)\bar{x}_j\right)M_m(\bar{x}_i)\bar{c}_{xm(n)}\right)\right]\right\} \quad (31)$$

According to the Hermite theorem,[23,24] the following auxiliary equations are also required

$$\sum_{j=1}^{np} N_{xj}(\bar{x}_i)\bar{c}_{j(n+1)}^k - \left[\sum_{j=1}^{np} N_{xj}(\bar{x}_i)\bar{x}_j\right]\sum_{m=1}^{np} M_m(\bar{x}_i)\bar{c}_{xm(n+1)}^k = 0 \quad (32)$$

$$\sum_{j=1}^{np} N_{xj}(\bar{x}_i)\bar{\psi}_{j(n+1)} - \left[\sum_{j=1}^{np} N_{xj}(\bar{x}_i)\bar{x}_j\right]\sum_{m=1}^{np} M_m(\bar{x}_i)\bar{\psi}_{xm(n+1)} = 0 \quad (33)$$

$$\sum_{j=1}^{npGel} N_{xj}(\bar{x}_i)\bar{u}_{j(n+1)} - \left[\sum_{j=1}^{npGel} N_{xj}(\bar{x}_i)\bar{x}_j\right]\sum_{m=1}^{npGel} M_m(\bar{x}_i)\bar{u}_{xm(n+1)} = 0 \quad (34)$$

$$\sum_{j=1}^{npGel} N_{xj}(\bar{x}_i)\bar{p}_{j(n+1)} - \left[\sum_{j=1}^{npGel} N_{xj}(\bar{x}_i)\bar{x}_j\right]\sum_{m=1}^{npGel} M_m(\bar{x}_i)\bar{p}_{xm(n+1)} = 0 \quad (35)$$

Simulating Results and Discussions

Numerical Validation of the MECe Model. By comparison with experimental data extracted from open literature, the computational accuracy of steady-state simulation of the MECe model has been validated for equilibrium analysis of the electric-sensitive hydrogels.[21,22] Further, a numerical comparison of transient simulation is made here with available experimental data. On the topic of kinetic experiment of the electric-sensitive hydrogels subject to external electric field, extensive search of the literature has thus far only found work published by Shiga et al.[26] In their experiment,[26] five kinds of PAA gels were prepared by free radical polymerization. One of them is used for the present validation, in which acrylic acid (AA, 0.1 mol), acrylamide (AAm, 0.1 mol), sodium hydroxide (0.06 mol), and N,N-methylene bisacrylamide (BAAm, 0.001 mol) were dissolved in distilled water. The total volume was 50 mL. After the addition of 50 mg of ammonium persulfate and 200 μL of N,N,N′,N′-tetramethylethylenediamine, the solution was poured into a plastic case and heated at 60 °C for 3 h for gelation. In a flask, 1 g of the prepared gel was immersed into 200 mL of distilled water until it reached swelling equilibrium with water. After the equilibrium, the gel was used as a specimen and distilled water as an aqueous solution. The aqueous solution was poured into a plastic case equipped with two parallel platinum electrodes. The specimen was placed in the center of the case, and the voltage was applied across the solution between the electrodes. As illustrated in Figure 2, they experimentally measured the endpoint displacement D of a hydrogel strip in a straightforward manner, instead of the displacement u at the edge point a of the present 1-D computational domain between the edge points a and b in the hydrogel thickness h direction along symmetric x-axis. A relation is thus required to link the two displacements D and u at different positions of the hydrogel strip. The experimental data[26] used as input data for the present numerical simulation include $T = 298$ (K), $R = 8.314$ (J/mol·K), $F_c = 9.648 \times 10^4$ (C/mol), $\epsilon = 80$, $\epsilon_0 = 8.854 \times 10^{-12}$ (C^2/Nm^2), $\phi_0^w = 0.8$, $c_0^f = 35.3$ (mol/m^3), $z^f = -1$, $c^* = 35.3$ (mol/m^3), $V_e = 3.0$ (V), $L = 5.0 \times 10^{-2}$ (m), $h = 5.0 \times 10^{-3}$ (m), and $3\lambda + 2\mu = 1.8 \times 10^4$ (Pa). The numerically computed displacement u and experimentally measured displacement D are tabulated in Table 1, at times $t = 1, 2, 3, 4,$ and 5 (min), respectively. The relation between the displacements u and D is constructed as a result of using the least-squares technique with best fitting to the displacements u and D at times $t = 1, 3,$ and 5 (min) only, and expressed by
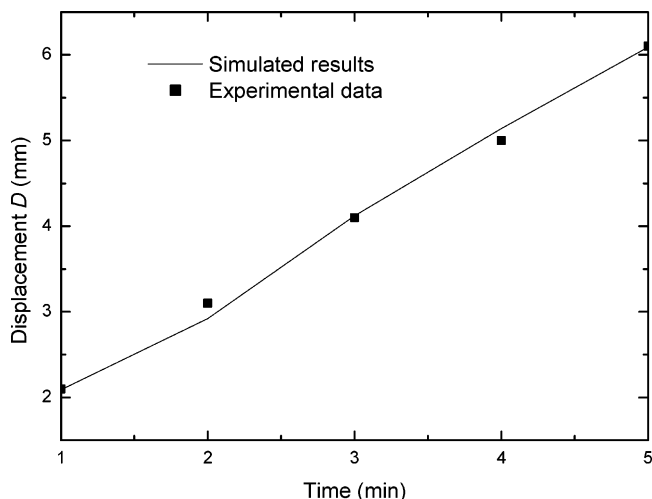
$$D = 1.58 + 0.93u + 0.47u^2 \quad (36)$$

Then, substituting the displacements u and D at times $t = 2$

CDV

Table 1. Displacements D and u at Different Times[a]

| time (min)	1	2	3	4	5
displacement D (mm)	2.1	3.1	4.1	5.0	6.1
displacement u (mm)	0.45	0.97	1.54	1.94	2.27

[a] D is the experimentally measured displacement at the endpoint of hydrogel strip. u is the displacement at the edge point a of the 1-D computational domain.

Figure 3. Comparison between the transiently simulated results and experimental data.

and 4 (min), respectively, into eq 36, the relative discrepancies are obtained and observed to be generally less than 6%. The relation (eq 36) is thus validated acceptable. Finally, for comparison of transient displacements D between experiment[26] and computation by eq 36, Figure 3 is produced, and very good agreement is observed for kinetics of the hydrogels. This validates the MECe model suitable for kinetics and equilibrium analyses of the electric-sensitive hydrogels.

Parameter Studies on Kinetics of the Hydrogels. To gain insight into kinetic behavior of the electric-stimulus responsive hydrogels, numerical simulations are made. Several parameters taken as input data in numerical implementation of the MECe model include $T = 298$ (K), $R = 8.314$ (J/mol·K), $F_c = 9.648 \times 10^4$ (C/mol), $\epsilon = 80$, $\epsilon_0 = 8.854 \times 10^{-12}$ (C^2/Nm^2), $\phi_0^w = 0.8$, $z^f = -1$, $3\lambda + 2\mu = 1.2 \times 10^5$ (Pa), $f_{ws} = 7.0 \times 10^{-16}$ (Ns/m^4), $D_k = 1.0 \times 10^{-7}$ (m^2/s), $L = 1.5 \times 10^{-2}$ (m), and $h = 5 \times 10^{-3}$ (m).

Concentration Kinetics of Ionic Species. The concentration kinetics of diffusive ion species are illustrated in Figures 4–11 for different electric fields V_e and fixed-charge densities c_0^f as well as bath solution concentrations c^*. Corresponding variations of the electric-stimulus responsive hydrogel with time are also presented. It is observed from the figures that, when no external electric field is applied at initial time $t = 0$, the concentration distributions of diffusive ions, resulting from the steady-state simulations, are symmetric in the entire computational domain. Once an external electric field V_e is imposed, the concentration distributions of the ionic species are no longer symmetric. The concentrations of diffusive ions redistribute continuously with time in both the hydrogel and the bath solution. The concentration differences near the hydrogel–solution interfaces increase with time. It is predictable that the ionic diffusion and convection will reach an equilibrium state after a specific time. The determination of this time is dependent on various material properties and environmental conditions, including the fixed-charge density c_0^f, external electric field V_e, and bath solution concentration c^*. It is also predictable from Figures 4–11 that
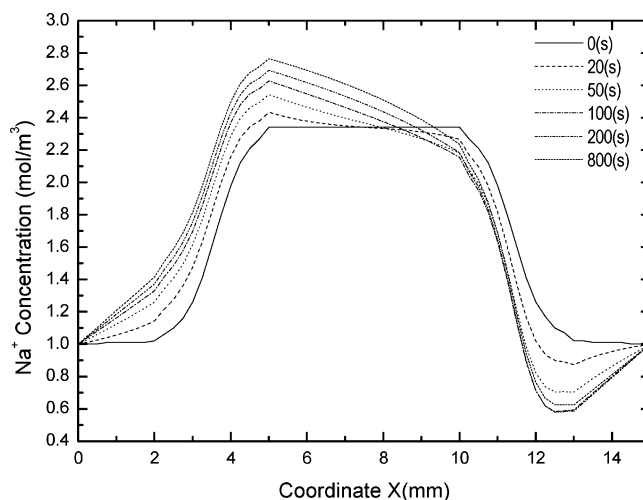
Figure 4. Na$^+$ concentration kinetics for $V_e = 0.2$ (V), $c_0^f = 2$ (mol/m^3), and $c^* = 1$ (mol/m^3).
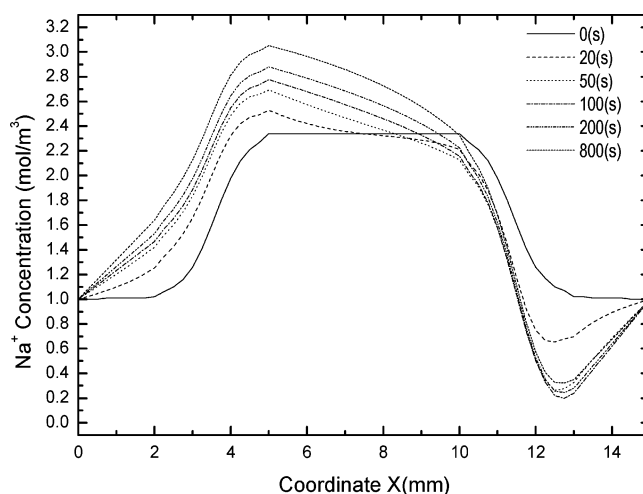
Figure 5. Na$^+$ concentration kinetics for $V_e = 0.4$ (V), $c_0^f = 2$ (mol/m^3), and $c^* = 1$ (mol/m^3).
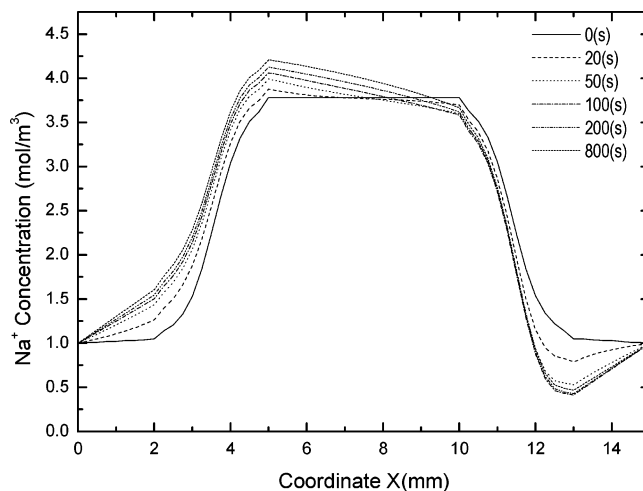
Figure 6. Na$^+$ concentration kinetics for $V_e = 0.2$ (V), $c_0^f = 4$ (mol/m^3), and $c^* = 1$ (mol/m^3).

the variations of distribution profiles of concentration kinetics with time will tend toward the steady-state FEM computational results.[19]

For discussion of influence of the externally applied electric voltage V_e on the distributions of concentration kinetics of diffusive ions, Figures 4 and 5 for the cation Na$^+$ and Figures
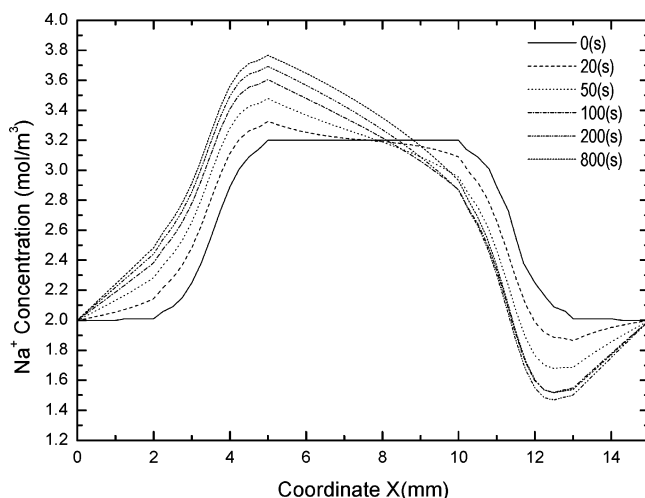
CDV

Figure 7. Na$^+$ concentration kinetics for $V_e = 0.2$ (V), $c_0^f = 2$ (mol/m^3), and $c^* = 2$ (mol/m^3).
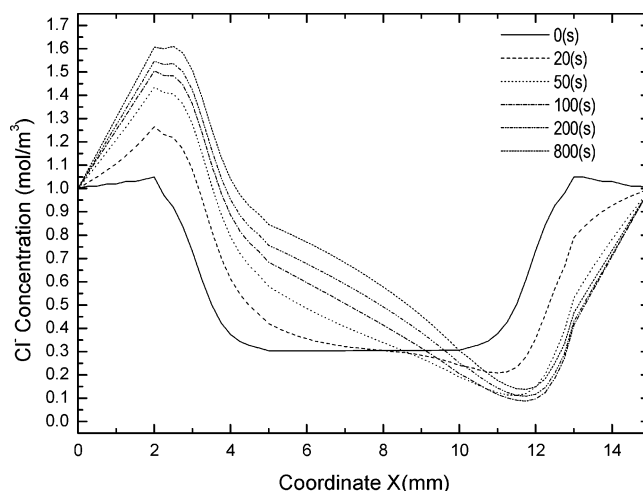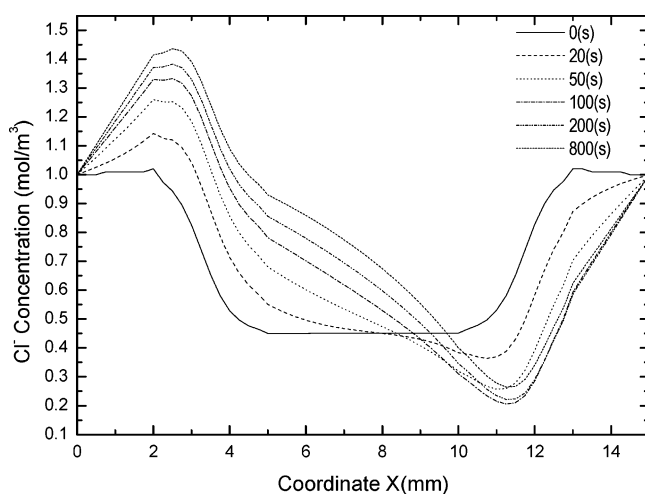

Figure 10. Cl$^-$ concentration kinetics for $V_e = 0.2$ (V), $c_0^f = 4$ (mol/m^3), and $c^* = 1$ (mol/m^3).

Figure 8. Cl$^-$ concentration kinetics for $V_e = 0.2$ (V), $c_0^f = 2$ (mol/m^3), and $c^* = 1$ (mol/m^3).
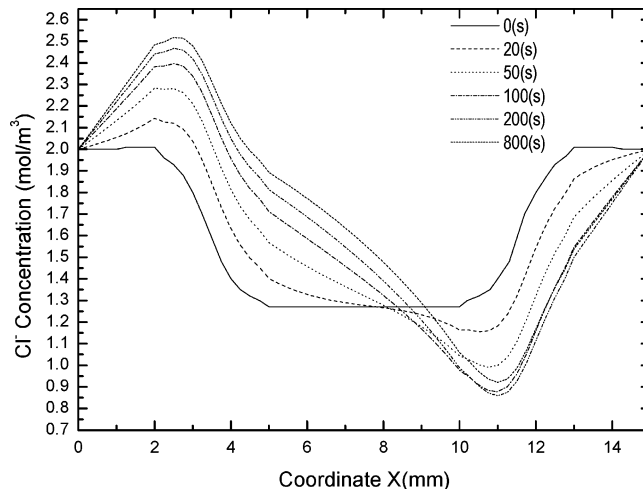

Figure 11. Cl$^-$ concentration kinetics for $V_e = 0.2$ (V), $c_0^f = 2$ (mol/m^3), and $c^* = 2$ (mol/m^3).
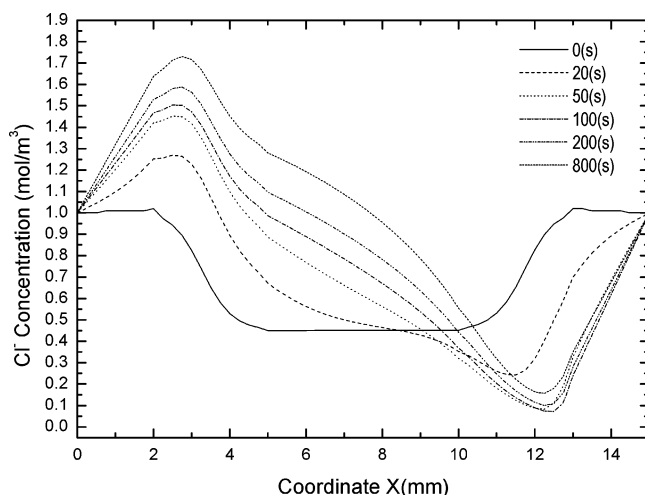

Figure 9. Cl$^-$ concentration kinetics for $V_e = 0.4$ (V), $c_0^f = 2$ (mol/m^3), and $c^* = 1$ (mol/m^3).

8 and 9 for the anion Cl$^-$ are examined, respectively. It is seen that, for the given fixed-charge density c_0^f and bath solution concentration c^*, the peak values of ionic concentrations on the hydrogel−solution interface near the cathode increase with increasing either time t or the applied electric voltage V_e, while those near the anode decrease. This reveals that the differences

of ionic concentrations between the two hydrogel−solution interfaces increase with time t or with the applied electric voltage V_e. It is foreseen that the variations of concentration distributions of the present transient simulations with time physically tend toward the steady-state concentration distributions by meshless simulations,[22] where the differences of ionic concentrations at equilibrium state increase as well with increasing the applied voltage V_e.

For analysis of influence of the fixed-charge density c_0^f on the kinetics of the hydrogels, Figures 4, 6, 8, and 10 are shown for the given electric voltage V_e and solution concentration c^*. The figures show that the variations of distributions of the concentration kinetics have similar characteristics to the steady-state simulations. With change of the fixed-charge density c_0^f, the variations of distributions of the cation Na$^+$ are significant with time t, while those of the anion Cl$^-$ are relatively insignificant. The reason may be the fixed-charge groups with negative valence. In addition, by comparing Figure 4 with Figure 7 for the cation Na$^+$ and Figure 8 with Figure 11 for the anion Cl$^-$, respectively, for the given electric voltage V_e and the fixed-charge densities c_0^f, the effect of bath solution concentration c^* is presented on the variations of concentration kinetics of diffusive ions. It is obviously found that the gradient of the concentration kinetics increases within the hydrogels, as the bath solution concentration c^* increases.
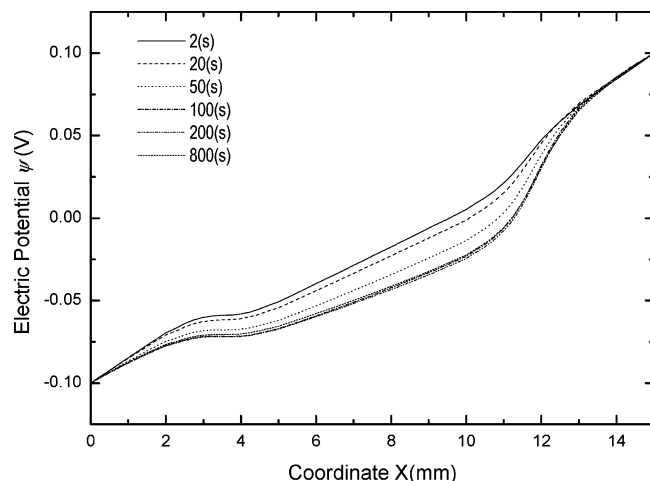
CDV

Figure 12. Variation of electric potential with time for $V_e = 0.2$ (V), $c_0^f = 2$ (mol/m³), and $c^* = 1$ (mol/m³).
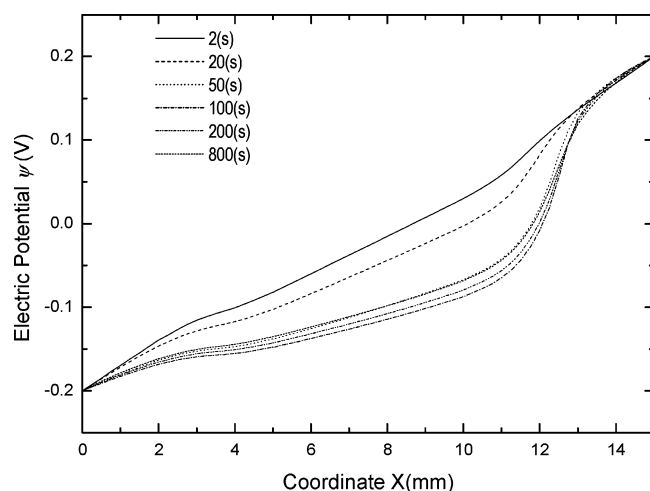

Figure 13. Variation of electric potential with time for $V_e = 0.4$ (V), $c_0^f = 2$ (mol/m³), and $c^* = 1$ (mol/m³).
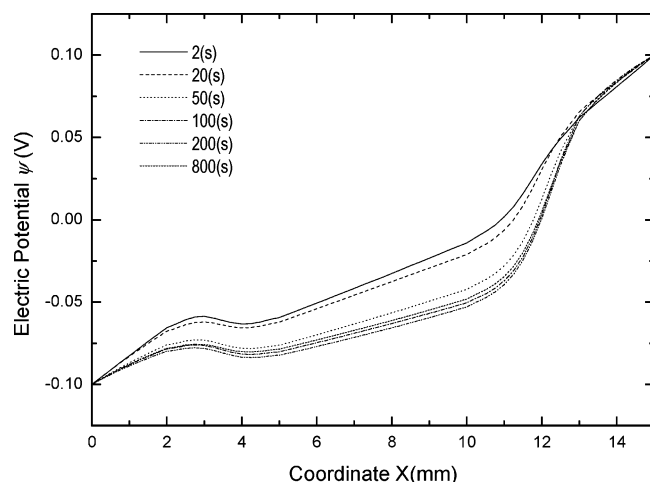

Figure 14. Variation of electric potential with time for $V_e = 0.2$ (V), $c_0^f = 4$ (mol/m³), and $c^* = 1$ (mol/m³).

Variation of Distribution of Electric Potential with Time. Figures 12−15 demonstrate the variation of distribution of the electric potential ψ with time for various combinations of environmental conditions including the applied electric voltage V_e and bath solution concentration c^* as well as fixed-charge density c_0^f. It is observed from the figures that the downward steps of distributions of the electric potential ψ within hydrogels
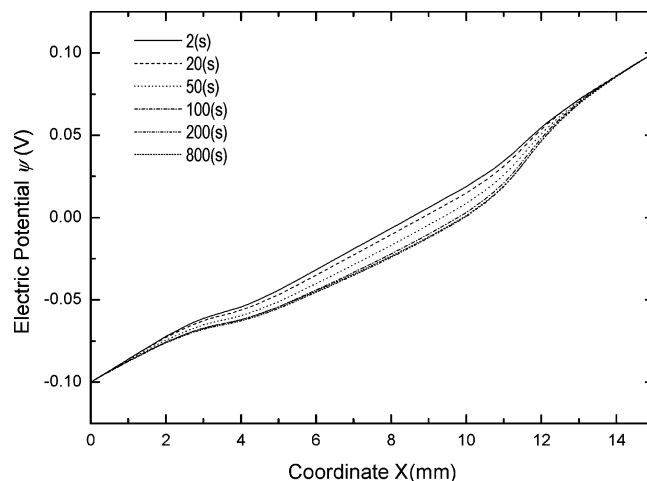

Figure 15. Variation of electric potential with time for $V_e = 0.2$ (V), $c_0^f = 2$ (mol/m³), and $c^* = 2$ (mol/m³).
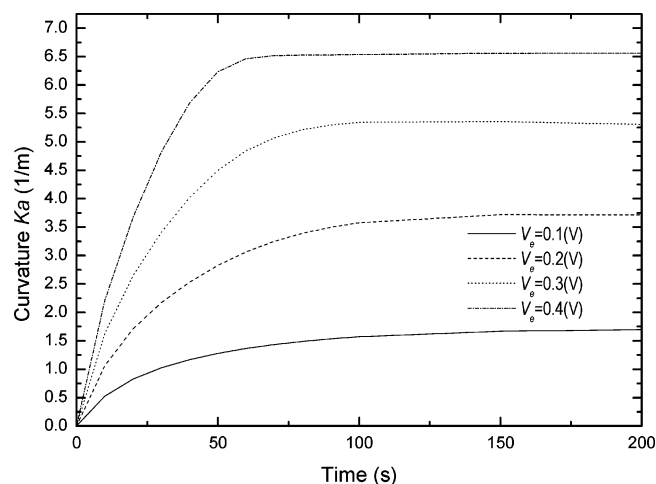

Figure 16. Effect of applied electric voltage V_e on variation of average curvature Ka with time.

increase with time. After a time of about 100 (s), the variation of the step becomes gradual. It is also found from Figures 12 and 13 that, with the increase of externally applied electric voltage V_e, the steps of distributions of the electric potential ψ on the hydrogel−solution interface near the cathode diminishes gradually, while those near the anode increase continuously. Figures 12 and 14 show that the effect of fixed-charge density c_0^f becomes less significant on the variation of distribution of electric potential with time. Probably, the reason is that the higher fixed-charge density c^f attracts more mobile ions into hydrogels and then results in the conductivity of the hydrogels closer to that of the surrounding bath solution.

Variation of Average Curvature of Hydrogel with Time. To describe the deformation of the electric-sensitive hydrogel, an important physical parameter, called average curvature Ka of the hydrogel, is defined as $Ka = 2(e_1 - e_2)/[h(2 + e_1 + e_2)]$, in which e_1 and e_2 are strains of the hydrogel at the edge points a and b in the thickness h direction of the hydrogel strip along symmetric x-axis (see Figure 2).[21,22] Figure 16 predicts the effect of the externally applied electric voltage V_e on kinetics of the average curvature Ka. For a given voltage V_e, the average curvature Ka first increases rapidly with time and subsequently in a more gradual manner. The average curvature Ka finally moves toward the steady-state solution after a critical time determined by the applied voltages V_e. It is observed that the critical time decreases with increasing the voltage V_e. Physically,
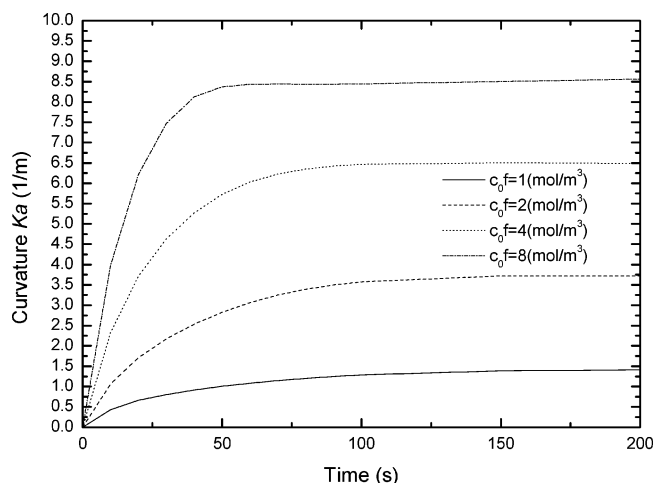
CDV

Figure 17. Effect of fixed-charge density c_0^f on variation of average curvature Ka with time.
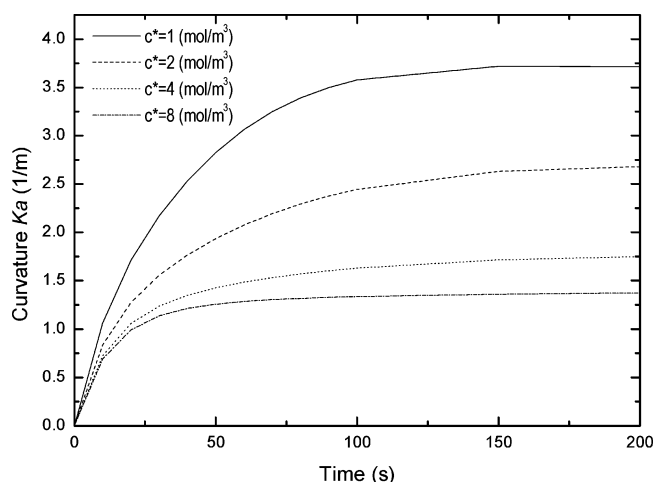

Figure 18. Effect of bath solution concentration c^* on variation of average curvature Ka with time.

the reason may be that the increase of the externally applied electric voltage V_e generates larger drag force to drive the diffusion of ionic species. This leads to a shorter time to reach the equilibrium state. In addition, at a given time t, the higher voltage V_e results in the larger average curvature Ka. It is because the stronger electric voltage V_e generates a larger difference in ionic concentrations between the hydrogel and the bath solution. The larger concentration difference induces higher osmotic pressure generating larger deformation of the hydrogels.

Figure 17 illustrates the influence of fixed-charge density c_0^f on the variations of average curvature Ka with time. Similarly, the average curvature Ka for a given fixed-charge density c_0^f first increases rapidly with time and then becomes gradual to come close to steady-state solution after a critical time. As shown in the figure, the critical time decreases with increasing the fixed-charge density c_0^f. Thus, the density c_0^f may be referred to as another driving source for ionic diffusion besides the externally applied electric field. It is found that, at a given time, the average curvature Ka increases with the increase of fixed-charge density c_0^f. The phenomenon is consistent with the published steady-state studies,[21,22] where the increase of fixed-charge density c_0^f makes larger deformation of the hydrogel.

Figure 18 demonstrates the influence of bath solution concentration c^* on the variation of average curvature Ka with time. A similar critical time is observed, and it decreases with

the increase of bath solution concentrations c^*. This implies that the bath solution concentration c^* has influence on the critical time. It is also illustrated in Figure 18 that, at a given time, the average curvature Ka decreases as the bath solution concentration c^* increases. This is consistent with the previous work,[22] in which the variation of diffusive ionic concentrations due to the fixed-charge density c_0^f is negligibly small if the bath solution concentration c^* is much larger than the fixed-charge density c_0^f.

On the basis of the above discussions of Figures 16−18, it is concluded that the average curvature Ka first increases rapidly with time and then in a more gradual manner. It reveals that the electric-sensitive hydrogels have the capability of responding very rapidly to external electric triggers. This is an important feature of the hydrogels and makes the hydrogels suitable for BioMEMS application as biosensors/bioactuators.

Conclusions

The transient simulation has been conducted by the MECe model for prediction of the kinetics of electric-stimulus responsive hydrogels. The model consisting of nonlinear coupled partial differential transient governing equations is validated suitable for kinetic analysis through the comparison of computed results with available experimental data. The model simulates the concentration kinetics of diffusive ionic species. The numerically transient results with time tend toward the published steady-state simulations. Influences of important parameters are also discussed, including the electric potential, fixed-charge density, bath solution concentration, and hydrogel average curvature. The transient simulation shows that the hydrogels are able to respond to the externally applied electric field in short time and indicate their great promise in BioMEMS applications.

References and Notes

(1) Jeong, B.; Gutowska, A. Lessons from nature: stimuli-responsive polymers and their biomedical applications. *Trends Biotechnol.* **2002**, *20*, 305−311.

(2) Galaev, I. Y.; Mattiasson, B. 'Smart' polymers and what they could do in biotechnology and medicine. *Trends Biotechnol.* **1999**, *17*, 335−340.

(3) Beebe, D. J.; Moore, J.; Bauer, J. M.; Yu, Q.; Liu, R. H.; Devadoss, C.; Jo, B.-H. Functional structures for autonomous flow control inside micro-fluidic channels. *Nature (London)* **2000**, *404*, 588−590.

(4) Li, H.; Ng, T. Y.; Yew, Y. K.; Lam, K. Y. Modeling and simulation of the swelling behavior of pH-stimulus-responsive hydrogels. *Biomacromolecules* **2005**, *6*, 109−120.

(5) Li, H.; Wang, X. G.; Yan, G. P.; Lam, K. Y.; Cheng, S. X.; Zou, T.; Zhuo, R. X. A novel multiphysic model for simulation of swelling equilibrium of ionized thermal-stimulus responsive hydrogels. *Chem. Phys.* **2005**, *309*, 201−208.

(6) Li, H.; Yew, Y. K.; Ng, T. Y.; Lam, K. Y. Meshless steady-state analysis of chemo-electro-mechanical coupling behavior of pH-sensitive hydrogel in buffered solution. *J. Electroanal. Chem.* **2005**, *580*, 161−172.

(7) Li, H.; Wang, X. G.; Wang, Z. J.; Lam, K. Y. Multiphysics modelling of volume phase transition of ionic hydrogels responsive to thermal stimulus. *Macromol. Biosci.* **2005**, *5*, 904−914.

(8) Li, H.; Wang, Z. J.; Wang, X. G.; Lam, K. Y. Simulation of the influences of bathing solution and crosslink density on the swelling

equilibrium of ionic thermo-sensitive hydrogels. *Biophys. Chem.* **2005**, *118*, 57−68.

(9) Li, H.; Yew, Y. K.; Lam, K. Y.; Ng, T. Y. Numerical simulation of pH-stimuli responsive hydrogel in buffer solutions. *Colloids Surf., A* **2004**, *249*, 149−154.

(10) Li, H.; Yan, G. P.; Wu, S. N.; Wang, Z. J.; Lam, K. Y. Numerical simulation of controlled nifedipine release from chitosan microgels. *J. Appl. Polym. Sci.* **2004**, *93*, 1928−1937.

(11) Wu, S. N.; Li, H.; Chen, J. P.; Lam, K. Y. Modeling investigation of hydrogel volume transition. *Macromol. Theory Simul.* **2004**, *13*, 13−29.

(12) Wu, S. N.; Li, H.; Chen, J. P. Modeling investigation of volume variation kinetics of fast response hydrogels. *J. Macromol. Sci., Part C:* **2004**, *44*, 113−130.

(13) Li, H.; Yuan, Z.; Ng, T. Y.; Lee, H. P.; Lam, K. Y.; Wang, Q. X.; Wu, S. N.; Fu, J.; Hanes, J. Constitutive model development and micro-structural topology optimisation for Nafion hydrogel membranes with ionic clustering. *J. Biomater. Sci., Polym. Ed.* **2003**, *14*, 1181−1196.

(14) Mow, V. C.; Kuei, S. C.; Lai, W. M.; Armstrong, C. G. Biphasic creep and stress relaxation of articular cartilage in compression: theory and experiments. *ASME J. Biomech. Eng.* **1980**, *102*, 73−84.

(15) Myers, E. R.; Lai, W. M.; Mow, V. C. A continuum theory and an experiment for the ion-induced swelling behavior of articular cartilage. *ASME J. Biomech. Eng.* **1984**, *106*, 151−158.

(16) Lanir, Y. Biorheology and fluid flux in swelling tissues. I. bicomponent theory for small deformations, including concentration effects. *Biorheology* **1987**, *23*, 173−188.

(17) Eisenberg, S. R.; Grodzinsky, A. J. The kinetics of chemically induced nonequilibrium swelling of articular cartilage and corneal stroma. *ASME J. Biomech. Eng.* **1987**, *109*, 79−89.

(18) Lai, W. M.; Hou, J. S.; Mow, V. C. A triphasic theory for the swelling and deformation behaviors of articular cartilage. *ASME J. Biomech. Eng.* **1991**, *113*, 245−258.

(19) Wallmersperger, T.; Kroplin, B.; Holdenried, J.; Gulch, R. W. A coupled multi-field formulation for ionic gels in electric fields. In *Proceedings of the SPIE 8th Annual International Symposium on Smart Structure and Materials*; Bar-Cohen, Y., Ed.; SPIE: Newport Beach, CA, 2001; Vol. 4329, pp 264−275.

(20) Zhou, X.; Hon, Y. C.; Sun, S.; Mak, A. F. T. Numerical simulation of the steady-state deformation of a smart hydrogel under an external electric field. *Smart Mater. Struct.* **2002**, *11*, 459−467.

(21) Li, H.; Yuan, Z.; Lam, K. Y.; Lee, H. P.; Chen, J.; Hanes, J.; Fu, J. Model development and numerical simulation of electric-stimulus-responsive hydrogels subject to an externally applied electric field. *Biosens. Bioelectron.* **2004**, *19*, 1097−1107.

(22) Li, H.; Chen, J.; Lam, K. Y. Multiphysical modeling and meshless simulation of electric-sensitive hydrogels. *J. Polym. Sci., Part B: Polym. Phys.* **2004**, *42*, 1514−1531.

(23) Li, H.; Ng, T. Y.; Cheng, J. Q.; Lam, K. Y. Hermite-cloud: a novel true meshless method. *Comput. Mech.* **2003**, *33*, 30−41.

(24) Li, H.; Cheng, J. Q.; Ng, T. Y.; Chen, J.; Lam, K. Y. A meshless Hermite-Cloud method for nonlinear fluid structure analysis of near-bed submarine pipelines under current. *Eng. Struct.* **2004**, *26*, 531−542.

(25) *An Introduction to the Finite Element Method*; Reddy, J. N., Ed.; McGraw-Hill: New York, 1993; pp 227−231.

(26) Shiga, T.; Karauchi, T. Deformation of polyelectrolyte gels under the influence of electric field. *J. Appl. Polym. Sci.* **1990**, *39*, 2305−2320.